

Primordial Black Hole Abundance from Reionization

Ziwen Yin,^{1,*} Hanyu Cheng,^{1,†} and Luca Visinelli^{2,3,‡}

¹*Tsung-Dao Lee Institute & School of Physics and Astronomy, Shanghai Jiao Tong University, Shanghai 201210, China*

²*Dipartimento di Fisica “E.R. Caianiello”, Università degli Studi di Salerno,*

Via Giovanni Paolo II, 132 - 84084 Fisciano (SA), Italy

³*Istituto Nazionale di Fisica Nucleare - Gruppo Collegato di Salerno - Sezione di Napoli,*

Via Giovanni Paolo II, 132 - 84084 Fisciano (SA), Italy

We derive robust constraints on the initial abundance of evaporating primordial black holes (PBHs) using the reionization history of the Universe as a cosmological probe. We focus on PBHs that inject electromagnetic (EM) energy into the intergalactic medium (IGM) after recombination, in the mass range $3.2 \times 10^{13} \text{ g} \lesssim M_{\text{PBH}} \lesssim 5 \times 10^{14} \text{ g}$. For each PBH mass, we compute the redshift-dependent energy injection from Hawking evaporation using `BlackHawk`, fully accounting for the time evolution of the PBH mass and the complete spectrum of emitted Standard Model particles and gravitons. The resulting photons and electrons are propagated through the primordial plasma using `DarkHistory`, which self-consistently models EM cascades and determines the fraction of injected energy deposited into ionization, excitation, and heating of the IGM. These modifications to the ionization and thermal histories are incorporated into a Gaussian Process reconstruction of the free-electron fraction based on low- ℓ CMB polarization data from the *Planck* mission. This non-parametric approach allows for a statistically well-defined separation between exotic high-redshift energy injection and late-time astrophysical reionization, allowing PBH evaporation to be constrained through its contribution to the high-redshift optical depth. Requiring consistency with current CMB measurements, we obtain upper limits on the initial PBH abundance that are robust against reionization modeling uncertainties and systematically more conservative than existing bounds, reflecting the fully numerical and time-dependent treatment of Hawking evaporation and energy deposition. Our results demonstrate the power of reionization observables as a precision probe of PBH evaporation and other scenarios involving late-time energy injection.

I. INTRODUCTION

Black holes (BHs) are among the most striking predictions of general relativity (GR), representing regions of spacetime where gravitational collapse leads to the formation of an event horizon. Over the past decades, compelling observational evidence has established their existence across a wide range of mass scales, including measurements of stellar orbits around Sagittarius A* at the Galactic Center [1–3], detections of gravitational waves (GW) from binary BH mergers [4, 5], and horizon-scale imaging of supermassive BHs in nearby galaxies [6, 7]. In the standard astrophysical picture, BHs form from the gravitational collapse of massive stars at the end of their life cycles [8].

In addition to these astrophysical objects, BHs may also have formed in the early Universe as primordial black holes (PBHs), generated by the collapse of large density fluctuations shortly after horizon re-entry [9–11]. Such fluctuations can arise in a variety of well-motivated scenarios, including enhanced curvature perturbations generated during inflation [12], modifications of the primordial equation of state [13], first-order phase transitions [14], scalar-mediated long-range forces [15], or bubble collisions in the early Universe [16, 17]. The

abundance of PBHs at formation is commonly estimated using Press–Schechter or peak-theory approaches, which require the density contrast to exceed a critical threshold $\delta_c \approx 0.4 - 0.7$ [18–22]. Comprehensive reviews of PBH formation and phenomenology can be found in Refs. [23–27].

A defining property of BHs is their emission of Hawking radiation due to quantum effects near the event horizon [28]. As a consequence, PBHs lose mass and eventually evaporate, with a lifetime that depends sensitively on their initial mass. PBHs heavier than $M_{\text{PBH}} \gtrsim 5 \times 10^{14} \text{ g}$ survive until the present epoch and have been extensively studied as potential dark matter (DM) candidates, constrained by microlensing [29], dynamical effects [30, 31], and cosmic microwave background (CMB) observations [32, 33], depending on their mass window. PBHs in the range $M_{\text{PBH}} \sim (10^{15} - 10^{17}) \text{ g}$ are additionally constrained by searches for gamma rays produced during their evaporation [34, 35]. PBHs with masses below $\sim 5 \times 10^{14} \text{ g}$ instead evaporate before the present epoch, injecting energy into the primordial plasma at redshifts between recombination and the onset of astrophysical reionization. In this regime, gamma-ray constraints rapidly weaken, while the ionization and thermal histories of the intergalactic medium (IGM) provides a sensitive probe of PBH evaporation. Astrophysical uncertainties in the timing and duration of reionization, however, can substantially weaken such bounds unless they are treated in a model-independent and data-driven manner. PBH evaporation has also been extensively studied as a possible mechanism for the non-thermal production of

* ziwenyin@sjtu.edu.cn

† chenghanyu@sjtu.edu.cn

‡ luvisinelli@unisa.it

DM candidates [36–44] and for its impact on axion production in the early Universe [45, 46]. In addition, the interplay between PBHs and DM halos surrounding them can lead to a variety of constraints on black hole and DM formation models [47–55]. While related effects often probe PBHs evaporating before or during Big-Bang nucleosynthesis, in this work we focus on later-evaporating PBHs whose dominant cosmological impact arises from energy injection into the IGM after recombination.

In this work, we study the cosmological impact of evaporating PBHs in the mass range $M_{\text{PBH}} \sim (10^{13}–10^{14}) \text{ g}$, which inject electromagnetic (EM) energy into the IGM after recombination and may partially evaporate up to the present epoch. PBHs in this mass window never dominate the energy density of the Universe and do not induce an early matter-dominated era. Instead, their cosmological signatures arise from late-time energy injection through Hawking radiation, leading to ionization, excitation, and heating of hydrogen and helium during the post-recombination epoch. These processes modify the ionization history and leave observable imprints on precision cosmological observables. Energy injection from evaporating PBHs has been previously constrained using CMB anisotropies [56–62], CMB spectral distortions [63–68], and global 21-cm measurements [69, 70]. Many of these analyses rely on semi-analytical treatments of the energy injection history or assume parametric models of reionization, which can obscure the separation between exotic energy injection and astrophysical reionization processes. Recently, a robust, data-driven framework for constraining late-time energy injection using reionization observables has been developed [71], in which the free-electron fraction is reconstructed directly from low- ℓ CMB polarization data using Gaussian Process (GP) regression. The corresponding numerical implementation is publicly available at github.com/Cheng-Hanyu/CLASS_reio_gpr. In this approach, this framework allows for constraints on exotic energy injection scenarios without imposing restrictive assumptions on the ionization history.

The goal of this work is to apply and extend this reionization methodology to evaporating PBHs in the mass range $(10^{13}–10^{14}) \text{ g}$. We model Hawking evaporation including the full set of relevant Standard Model degrees of freedom, track the resulting time-dependent energy injection and EM cascades in the IGM, and derive constraints on the initial PBH abundance, commonly parametrized by the mass fraction at formation β . Our analysis follows a strategy similar to that developed for ensembles of decaying relics [72], adapted here to the intrinsically time-dependent nature of PBH evaporation. We show that reionization observables provide competitive and complementary constraints in this mass window, highlighting the unique sensitivity of the ionization history to late-time energy injection.

The paper is organized as follows. In Sec. II we review the formation and evaporation of PBHs, describe the computation of their Hawking emission spectra, and

outline the cosmological framework used to model energy injection and EM cascades in the IGM. In Sec. III we present the analysis pipeline, detailing the treatment of the ionization and thermal histories, the GP reconstruction of the reionization history, and the extraction of constraints from the high-redshift optical depth. Our results are presented in Sec. IV, where we derive bounds on the initial PBH abundance as a function of mass, and are discussed in Sec. V through comparisons with existing constraints and an assessment of the physical effects. We summarize our findings and outline future prospects in Sec. VI. Throughout this work we use natural units $\hbar = c = k_B = 1$, and we refer to the Planck mass in terms of Newton's constant G_N as $m_{\text{Pl}} = G_N^{-1/2}$.

II. METHODS

PBHs are characterized by their initial abundance, typically defined as the fraction of the Universe's energy density that collapses into black holes at the time of formation t_f ,

$$\beta = \frac{8\pi G_N}{3H^2(t_f)} \rho_{\text{PBH}}(t_f), \quad (1)$$

where ρ_{PBH} is the PBH energy density and $H(t)$ is the Hubble rate at time t . In the absence of evaporation, the PBH energy density scales as matter and grows relative to radiation until matter-radiation equality. It is convenient to relate β to an effective PBH fraction of dark matter at equality, f_{PBH} , using entropy conservation during radiation domination,

$$\beta = f_{\text{PBH}} \left(\frac{g_{*s}(T_{\text{eq}})}{g_{*s}(T_f)} \right)^{1/3} \frac{T_{\text{eq}}}{T_f}. \quad (2)$$

Throughout this work we quote constraints in terms of β , which remains well-defined even when PBHs evaporate before matter-radiation equality.

In the standard scenario, PBHs form during radiation domination from the collapse of overdense regions [10, 11]. Assuming a monochromatic mass function, the PBH mass at formation is related to the horizon mass by a collapse efficiency factor $\gamma \simeq 0.2$,

$$M_{\text{PBH}} = \gamma \frac{4\pi}{3} \frac{\rho_{\text{crit}}(t_f)}{H_f^3} = \frac{\gamma}{2G_N H_f}, \quad (3)$$

where $H_f \equiv H(t_f)$. In our analysis, the PBH mass M_{PBH} and initial abundance β are treated as independent parameters.

When evaporation is neglected, the comoving number density of PBHs at redshift z corresponding to an effective fraction f_{PBH} of DM is

$$n_{\text{PBH}}(M_{\text{PBH}}, z) = f_{\text{PBH}} \frac{\rho_c \Omega_{\text{DM}}}{M_{\text{PBH}}} (1+z)^3, \quad (4)$$

where $\rho_c \equiv 3H_0^2/(8\pi G_N)$ is the present-day critical density, which depends on the value of the Hubble constant H_0 , and Ω_{DM} is the present-day dark matter density parameter. For the PBH masses considered in this work, however, Hawking evaporation proceeds over cosmological timescales, and the PBH mass evolves appreciably between recombination and reionization. PBHs lose mass through Hawking evaporation, emitting all particle species with masses below the Hawking temperature [73–75]

$$T_H = \frac{1}{8\pi G_N M_{\text{PBH}}}. \quad (5)$$

We assume that PBHs with masses $M_{\text{PBH}} \sim (10^{13}\text{--}10^{14})\text{ g}$, formed from near-spherical collapse during radiation domination, are well approximated as non-spinning [76, 77]. The total mass loss rate of a non-rotating PBH is given by

$$\frac{dM_{\text{PBH}}}{dt} = - \sum_i \int dE E \frac{d^2 N_i}{dE dt}(E; M(t)), \quad (6)$$

where the sum runs over all particle species i . The emission rate for the i -th degrees of freedom with spin s_i and internal degrees of freedom g_i , per unit time and energy is given as

$$\frac{d^2 N_i}{dE dt}(E; M(t)) = \sum_{\ell} \frac{g_i}{2\pi} \frac{\Gamma_{s_i, \ell}(E)}{e^{E/T_H} \pm 1}, \quad (7)$$

where $\Gamma_{s_i, \ell}(E)$ denotes the graybody factor encoding the probability for a mode of energy E and angular momentum ℓ to escape the BH potential barrier [78]. For non-rotating PBHs, these graybody factors are obtained by solving the Bardeen-Press equation for each spin [74, 79–81]. While the PBH lifetime scales parametrically as $\tau \propto M_{\text{PBH}}^3$, accurate modeling of the evaporation history requires numerical integration of the mass loss rate, particularly near the end of the PBH lifetime when the emission rate increases rapidly.

In this work, we compute the full time evolution of the PBH mass by numerically evolving the mass loss Eq. (6) using the `BlackHawk 2.3` code [82–84], including all relevant SM degrees of freedom as well as gravitons. This fully time-dependent treatment is essential for accurately modeling the redshift distribution of energy deposition, particularly near the end of the PBH lifetime, when the emission rate increases rapidly and can significantly affect the ionization history of the IGM. The instantaneous PBH mass $M_{\text{PBH}}(t)$ is used to evaluate the emitted particle spectra and energy injection rate at each redshift. Primary spectra for photons and electrons/positrons are obtained directly from `BlackHawk 2.3`, while secondary EM emission from particle decays and final-state radiation is computed using `HAZMA` [85], a code designed to model EM emission from particle injection in astrophysical environments at late times. Given the emission rate

for photons and electrons, the total injected EM energy density per unit physical volume and time is

$$\left(\frac{dE}{dV dt} \right)_{\text{inj}}(z) = n_{\text{PBH}} \sum_{i \in \{\gamma, e^{\pm}\}} \int dE E \frac{d^2 N_i}{dE dt}(E; M(t)). \quad (8)$$

Injected photons and electrons initiate EM cascades through Compton scattering, inverse Compton scattering, pair production, and photoionization. Because of these processes, energy deposition does not occur instantaneously and must be treated self-consistently. In the following, we convert the time derivative in Eq. (8) into a redshift dependence, with the sign convention imposed such that a positive value corresponds to net heating of the baryonic gas.

III. ANALYSIS

A. Ionization of the IGM by PBH evaporation

We analyze the impact of PBH Hawking evaporation on the thermal and ionization history of the IGM between recombination and the onset of astrophysical reionization. In this regime the ionization history is primarily governed by standard recombination physics, but it can be modified by additional sources of energy injection such as the EM products of PBH evaporation. During this epoch, the free-electron fraction evolves under the combined action of recombination processes and any additional injected energy. The ionization state of the IGM is characterized by the ionization fraction

$$X_e \equiv \frac{n_e}{n_H}, \quad (9)$$

where n_e is the number density of free electrons and n_H is the total number density of hydrogen nuclei. The kinetic temperature of the baryonic gas T_b is defined in terms of the mean thermal energy per particle,

$$\frac{3}{2} k_B T_b = \langle \frac{1}{2} m_b v^2 \rangle, \quad (10)$$

where m_b is the mass of the specific baryon considered and the average account for its momentum distribution. The evolution of X_e and T_b is described by the coupled differential equations [86, 87]

$$\begin{aligned} \frac{dX_e}{dz} &= \frac{C_H}{(1+z)H(z)} \left(-\beta_H(T_\gamma)(1-X_e) e^{-\frac{E_{H,2s1s}}{T_\gamma}} + X_e^2 n_H \alpha_H(T_b) \right) \\ &+ \frac{1}{n_H E_i} \frac{dE}{dV dz} \bigg|_{\text{dep,ion}} + (1-C_H) \frac{1}{n_H E_{H,1s2p}} \frac{dE}{dV dz} \bigg|_{\text{dep,exc}}, \end{aligned} \quad (11)$$

$$\begin{aligned} (1+z) \frac{dT_b}{dz} &= 2T_b + \frac{8}{3} \frac{\rho_\gamma \sigma_T}{m_e H(z)} \frac{X_e}{1+f_{\text{He}}+X_e} (T_b - T_\gamma) \\ &+ \frac{2}{3} \frac{1+z}{n_H (1+f_{\text{He}}+X_e)} \frac{dE}{dV dz} \bigg|_{\text{dep,heat}}. \end{aligned} \quad (12)$$

Here, T_γ is the photon temperature, related to the photon energy density by $\rho_\gamma = (\pi^2/15)T_\gamma^4$, and σ_T is the Thomson cross section. The coefficients α_H and β_H denote the case-B recombination and photoionization rates, respectively. The hydrogen excitation and ionization energies are $E_{H,1s2p} = E_{H,2s1s} = 10.2$ eV and $E_i = 13.6$ eV, and f_{He} is the helium-to-hydrogen number density ratio. The Peebles factor C_H accounts for the probability that an excited hydrogen atom reaches the ground state before being ionized. At high redshift, baryons remain tightly coupled to photons through efficient Compton scattering, so that $T_b = T_\gamma$. After recombination, Compton coupling weakens and the baryon temperature evolves approximately adiabatically, with $T_\gamma \propto (1+z)$ and $T_b \propto (1+z)^2$, leading to a decreasing ratio T_b/T_γ around $z \sim 200$ –1000. Any additional heating source such as PBH evaporation modifies this post-recombination thermal evolution through the extra terms in Eqs. (11)–(12).

Energy injected into the IGM by PBH evaporation is redistributed among ionization, excitation, and heating channels, labeled by $c = \{\text{ion, exc, heat}\}$. The impact of exotic energy injection is fully characterized by the rate at which energy is deposited into the baryon-photon plasma as a function of redshift [56–60]. For each channel c , the deposited energy rate per unit time is

$$\frac{dE}{dV dt} \Big|_{\text{dep},c}(z) = f_c(z) \left(\frac{dE}{dV dt} \right)_{\text{inj}}(z), \quad (13)$$

where $f_c(z)$ is the redshift-dependent deposition efficiency computed using `DarkHistory` [88], which propagates the injected photon and electron spectra through EM cascades in the expanding Universe. Following Ref. [60], we write

$$f_c(z) = \chi_c f(z), \quad (14)$$

where the function χ_c depends on X_e [58, 89, 90], while the redshift-dependent expression reads

$$f(z) = \frac{\sum_{i \in \{\gamma, e^\pm\}} \int dE E \frac{d^2 N_i}{dE dt} f_i(E, z)}{\sum_{i \in \{\gamma, e^\pm\}} \int dE E \frac{d^2 N_i}{dE dt}}. \quad (15)$$

Here, $f_i(E, z)$ are the species- and energy-dependent deposition probabilities obtained from detailed cascade simulations [91, 92]. This procedure fully accounts for the coupled evolution of photon and electron cascades. The resulting deposited energy rate serves as the source term for the ionization and thermal evolution in Eqs. (11)–(12). In the absence of significant helium reionization, the total hydrogen number density is expressed as

$$n_H = n_e + n_{HI} = 3.1 \times 10^{-8} \eta_{10} \left(\frac{T_\gamma}{T_{\gamma 0}} \right)^3 \text{ cm}^{-3}, \quad (16)$$

where n_{HI} is the neutral hydrogen density, $\eta_{10} = 10^{10} n_b / n_\gamma \simeq 6.1$ is the baryon-to-photon ratio [93], and $T_{\gamma 0} \simeq 2.725$ K is the present-day photon temperature. The photon temperature evolves as

$$T_\gamma = T_{\gamma 0} (1+z). \quad (17)$$

While our primary focus is the modification of the ionization history at high redshifts due to PBH evaporation, the computation of observables such as the Thomson optical depth requires a complete ionization history down to low redshift. At redshifts $z \lesssim 30$, the ionization state of the IGM is dominated by astrophysical sources such as stars and galaxies. We model this phase using a hyperbolic tangent parametrization [94],

$$X_{\text{rei}}(z) = \frac{1+f_{\text{He}}}{2} \left[1 + \tanh \left(\frac{(1+z_{\text{re}})^{3/2} - (1+z)^{3/2}}{(3/2)(1+z)^{1/2}\Delta z} \right) \right], \quad (18)$$

with $z_{\text{re}} = 6.1$ and $\Delta z = 0.5$. The helium-to-hydrogen number density ratio is

$$f_{\text{He}} = \frac{n_{\text{He}}}{n_H} = \frac{Y_p}{4(1-Y_p)}, \quad (19)$$

where Y_p is the primordial helium mass fraction. The full ionization history is then the sum of the quantity obtained from the modified recombination equations, including PBH energy injection, and a phenomenological contribution from late-time astrophysical reionization, so that the total free-electron fraction entering the optical depth calculation in Eq. (21) below is

$$X_e^{\text{tot}}(z) = X_e(z) + X_{\text{rei}}(z). \quad (20)$$

Here, we keep referring to the reionization history as $X_e(z)$.

B. Optical depth decomposition and high-redshift constraints

The modified ionization history induced by PBH evaporation impacts the CMB primarily via the Thomson optical depth,

$$\tau(z) = \int_0^z dz' \frac{c n_e(z') \sigma_T}{(1+z') H(z')}. \quad (21)$$

Following Ref. [71], we decompose the total optical depth into low- and high-redshift contributions, $\tau = \tau_{\text{lowz}}(z_c) + \tau_{\text{highz}}(z_c)$. The transition redshift z_c allows for a clean separation between the ionization contribution from known astrophysical reionization sources, such as stars and galaxies, which dominate at $z < z_c$, and that from exotic energy injection at higher redshifts. We focus exclusively on $\tau_{\text{highz}}(z_c)$ to constrain the PBH parameter space. We set $z_c = 30$ and adopt a robust constraint derived from a GP reconstruction of the reionization history $X_e(z)$ using *Planck* 2018 low- ℓ polarization data [71]. Specifically, that analysis performs Bayesian inference using the low- ℓ EE-only SimAll likelihood from the *Planck* 2018 data release [95, 96], implemented in `Cobaya` [97] and coupled to a modified version of `CLASS` [98] supporting non-parametric $X_e(z)$ reconstructions up to $z_{\text{max}} = 800$. Standard Λ CDM parameters are fixed to their *Planck* 2018 best-fit values so that

the inferred τ_{highz} posterior is determined primarily by the low- ℓ polarization data.

We also restrict the PBH-induced energy injection to be post-recombination and within the redshift range covered by the GP reconstruction. We adopt $z_{\text{max}} \simeq 800$ as a conservative upper limit: for injections approaching recombination, modifications to $X_e(z)$ primarily deform the visibility function around last scattering and become increasingly degenerate with recombination-era physics and standard cosmological parameters (such as n_s or Y_p), limiting the robustness of constraints derived from low- ℓ polarization alone. We therefore focus on the interval $30 \leq z \leq 800$. This redshift window defines the PBH mass interval

$$3.2 \times 10^{13} \text{ g} \lesssim M_{\text{PBH}} \lesssim 5 \times 10^{14} \text{ g}, \quad (22)$$

corresponding to Hawking temperatures

$$330 \text{ MeV} \gtrsim T_H \gtrsim 21 \text{ MeV}. \quad (23)$$

The lower mass limit corresponds to PBHs that fully evaporate by z_{max} , ensuring their energy injection is treated consistently as a perturbation to the optical depth rather than a modification to the recombination history. The upper limit corresponds to PBHs evaporating at the present day, which inject energy continuously throughout the post-recombination epoch. The EM cascades from these evaporating PBHs are modeled using `BlackHawk` and `DarkHistory`, accounting for the prompt hadronization and decay of primary particles.

IV. RESULTS

Within the mass window defined in Eq. (22), we assume a monochromatic PBH mass function and generate complete evaporation histories at representative mass points, spaced by $\Delta M_{\text{PBH}} = 1.6 \times 10^{13} \text{ g}$ across the mass interval in Eq. (22). Each mass point is treated independently, providing a full time-dependent emission history analogous to scanning over different particle physics scenarios for the injected spectra.

Figure 1 shows the resulting constraints on the initial PBH mass fraction at formation, β , as a function of the PBH mass, obtained from the effects of Hawking evaporation on the thermal and ionization history of the Universe at 95% confidence level (C.L.). The upper bound on β is obtained by requiring consistency with the posterior distribution of the high-redshift contribution to the Thomson optical depth, τ_{highz} , see Fig. 2 in Ref. [71], ensuring that the additional energy deposition does not overionize the IGM or excessively heat the baryonic gas. The resulting constraint exhibits a mild nonlinear dependence on the PBH mass. Heavier PBHs inject energy at later times, so the resulting increase in the free-electron fraction occurs predominantly at lower redshifts. Because the optical-depth integral in Eq. (21) is weighted toward

higher redshift, $\tau(z) \propto \int_0^z dz' X_e(z') (1+z')^{1/2}$, ionization occurring at late times is less efficient at enhancing $\tau(z)$, leading to weaker constraints. In addition, as the Hawking temperature increases toward lower PBH masses, the opening of hadronic and heavier SM emission channels redistributes the PBH luminosity among all species. After folding in hadronization, decays, and EM cascades from the PBH evolution and the particles propagation codes, this redistribution reduces the effective EM branching ratio, defined as the fraction of the total Hawking power that ultimately appears in photons and electrons/positrons and can efficiently couple to the IGM. This suppresses the impact of lighter PBHs on reionization observables and contributes to the weakening of the constraint at the low-mass end of the window.

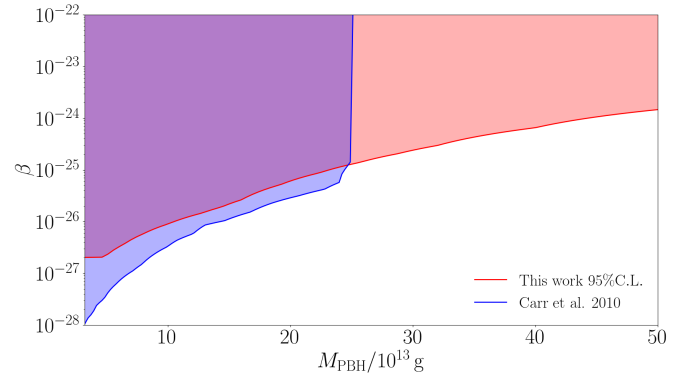


FIG. 1. Upper bounds at 95% C.L. on the initial PBH mass fraction at formation, β , as a function of the PBH mass for non-spinning black holes. The mass range shown corresponds to PBHs whose EM energy injection occurs predominantly at redshifts $z < z_{\text{max}}$. The constraints are derived from the impact of Hawking evaporation on the thermal and ionization history of the IGM, as inferred from the high-redshift optical depth.

Our results in Fig. 1 are compared with the CMB-based constraints derived in Ref. [23]. In that work, bounds in the mass range $M_{\text{PBH}} \sim 10^{13}\text{--}10^{14} \text{ g}$ are primarily driven by the damping of CMB temperature anisotropies due to energy injection around recombination, modeled using analytic estimates of the PBH lifetime and simplified prescriptions for energy deposition.¹ By contrast, the constraints presented here rely on a fully time-dependent numerical treatment of PBH evaporation and EM cascades, and are derived from the reconstructed high-redshift optical depth using a GP approach that is explicitly insensitive to late-time astrophysical reionization [71]. This strategy allows us to isolate the contribution of exotic energy injection at $z \gtrsim 30$ and to

¹ Other works have also derived CMB anisotropy constraints on light PBHs using increasingly detailed energy injection and recombination modeling, including comprehensive treatments of EM cascades and Boltzmann evolution [60–62, 66].

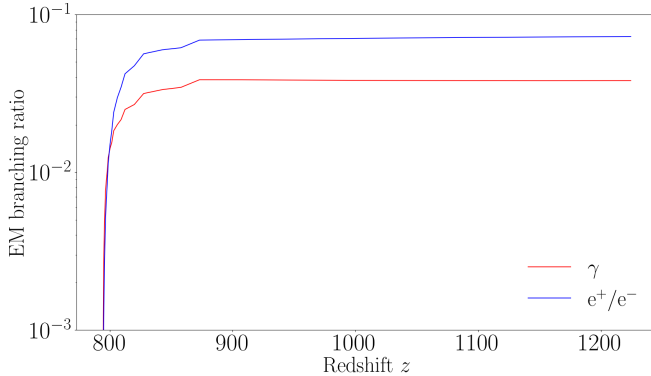


FIG. 2. Time evolution of the effective EM branching ratio into photons (red) and electrons/positrons (blue) for PBH evaporation with mass $M_{\text{PBH}} = 3.2 \times 10^{13} \text{ g}$ and initial abundance $\beta = 1.6 \times 10^{-27}$. The EM branching ratio is defined as the fraction of the total Hawking luminosity that ultimately appears in electromagnetically interacting particles after hadronization, decays, and secondary EM cascades.

probe PBH evaporation effects extending beyond the recombination epoch. As a result, our bounds provide a complementary constraint on the initial PBH abundance based on the improved sensitivity of modern high-redshift ionization measurements, providing a robust constraint complementary to earlier CMB limits. At the lowest PBH masses, our bounds are weaker than those of Ref. [23] because a fully time-dependent treatment of Hawking evaporation and EM cascades shows that an increasing fraction of the PBH luminosity is carried by non-EM interacting particles and by high-energy photons that deposit their energy inefficiently at $z \lesssim 800$, an effect that is not captured by instantaneous injection approximations. In fact, the effective EM branching ratio, obtained after consistently accounting for both the primary Hawking emission spectrum and the full secondary particle production, including hadronization and decays, is strongly mass- and redshift-dependent, as shown in Fig. 2 for a PBH of mass $3.2 \times 10^{13} \text{ g}$ evaporating at $z \simeq 800$. At low PBH masses, additional emission channels reduce the fraction of energy in photons and electrons, partially relaxing previous bounds that assumed a fixed EM fraction. The branching ratio evolution, combined with the full time-dependent emission treatment, explains the observed mild suppression of constraints in the low-mass regime of Fig. 1.

V. DISCUSSIONS

The time-dependent emission histories allow us to study the detailed impact of PBH evaporation on the IGM and baryon-photon plasma. Figure 3 shows the evolution of the hydrogen ionization fraction, $X_e(z)$, for PBHs of different masses near their respective upper bounds on the initial PBH mass fraction β , compared to the baseline ΛCDM evolution. For PBH masses $M_{\text{PBH}} \gtrsim$

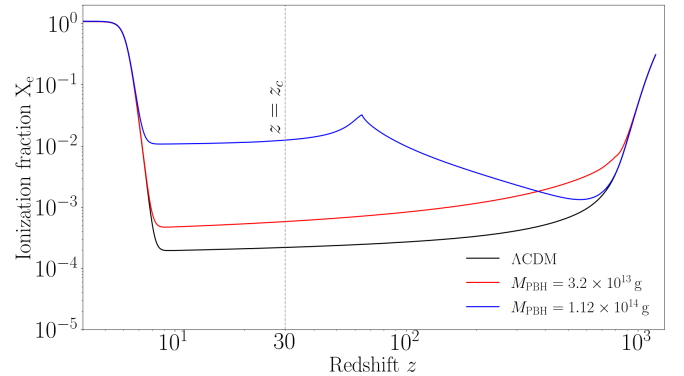


FIG. 3. Hydrogen ionization fraction $X_e(z)$ as a function of redshift for two representative PBH populations evaluated near their respective upper limits on the initial PBH mass fraction β : $M_{\text{PBH}} = 3.2 \times 10^{13} \text{ g}$ (red) and $M_{\text{PBH}} = 1.12 \times 10^{14} \text{ g}$ (blue). The black solid line shows the baseline ΛCDM ionization history.

$3.2 \times 10^{13} \text{ g}$, evaporation occurs at redshifts $z < z_{\text{max}}$, producing a characteristic spike in $X_e(z)$ at the epoch when most of the EM energy is injected into the IGM. In the figure and in the followings, we show two representative PBH populations: one with $M_{\text{PBH}} = 3.2 \times 10^{13} \text{ g}$ and $\beta = 1.6 \times 10^{-27}$, corresponding to PBHs that evaporate close to the maximum redshift considered in our analysis, and a second with $M_{\text{PBH}} = 1.12 \times 10^{14} \text{ g}$ and $\beta = 1.4 \times 10^{-26}$, representative of heavier PBHs that evaporate at later times. In both cases, the chosen values of β lie close to the corresponding upper limits derived from the optical depth constraint, and are illustrative of the maximal ionization signatures consistent with current data.

The amplitude of the resulting spike in $X_e(z)$ is modulated by the EM branching ratio, which is computed numerically from the full Hawking emission spectrum and accounts for the suppression of EM energy at earlier evaporation times, when a larger fraction of the emitted power is carried by non-interacting particles. PBHs can substantially modify the ionization history of the Universe during the post-recombination epoch. While our analysis uses the high-redshift optical depth τ_{highz} as a derived constraint, a direct χ^2 comparison against the GP reconstruction of $X_e(z)$ itself would, in principle, be sensitive to the detailed spike structure and could yield slightly tighter bounds on PBH abundances. By contrast, the current approach is conservative, as τ_{highz} effectively integrates over the ionization history and does not fully exploit transient enhancements in X_e at specific redshifts.

We now focus on the impact of a population of PBHs of mass $M_{\text{PBH}} = 3.2 \times 10^{13} \text{ g}$, thus evaporating around redshift $z = 800$ which is taken here as the maximum redshift considered in the reionization reconstruction. We fix the initial abundance of this population as $\beta = 1.6 \times 10^{-27}$, corresponding to a DM fraction in PBH of $f_{\text{PBH}} \approx 5 \times 10^{-9}$. Figure 4 illustrates how the GP constraint on the high-redshift optical depth translates into

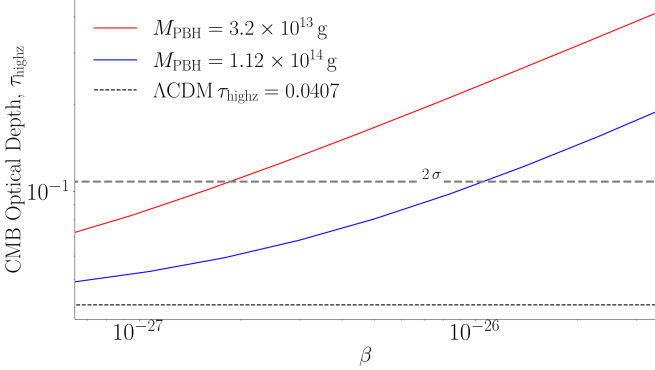


FIG. 4. High-redshift CMB optical depth τ_{highz} induced by PBH evaporation as a function of the initial PBH mass fraction β . The red solid line corresponds to PBHs with mass $M_{\text{PBH}} = 3.2 \times 10^{13} \text{ g}$, while the blue solid line corresponds to $M_{\text{PBH}} = 1.12 \times 10^{14} \text{ g}$. For each mass, τ_{highz} is obtained by integrating the modified ionization history resulting from the full time-dependent Hawking evaporation and EM energy deposition into the IGM at redshifts above z_c . The black dashed line denotes the ΛCDM baseline contribution in the absence of PBHs. The horizontal gray dashed line indicates the 95% C.L. upper limit on τ_{highz} inferred from the GP reconstruction of the reionization history in Ref. [71]. The intersection of this bound with each colored curve determines the corresponding upper limit on β .

an upper limit on the initial PBH abundance. The figure shows the contribution to the high-redshift CMB optical depth, τ_{highz} , as a function of the initial PBH mass fraction β for two representative PBH masses. For each value of β , the optical depth is obtained by integrating the modified ionization history $X_e(z)$ resulting from the full, time-dependent Hawking evaporation of PBHs and the subsequent EM energy deposition into the IGM. The increase of τ_{highz} with β reflects the fact that a larger initial PBH abundance leads to a higher energy injection rate and hence to an enhanced free-electron fraction over the post-recombination epoch. The dependence on PBH mass arises from the redshift at which most of the evaporation power is released and from the evolving EM branching ratio. Lighter PBHs evaporate earlier and inject a larger fraction of their energy at higher redshift, producing a more rapid increase in τ_{highz} for a given β . Heavier PBHs evaporate more slowly, leading to a more extended and less efficient contribution to the high-redshift optical depth. The black dashed line indicates the ΛCDM baseline contribution to τ_{highz} in the absence of PBHs, while the horizontal gray dashed line denotes the 95% confidence-level upper limit inferred from the GP reconstruction of the reionization history [71]. Requiring the PBH-induced contribution to remain below this bound yields an upper limit on β , determined by the intersection of each curve with the gray dashed line. This procedure provides a direct and model-independent mapping between the GP-derived reionization constraint and the PBH parameter space, without relying on specific as-

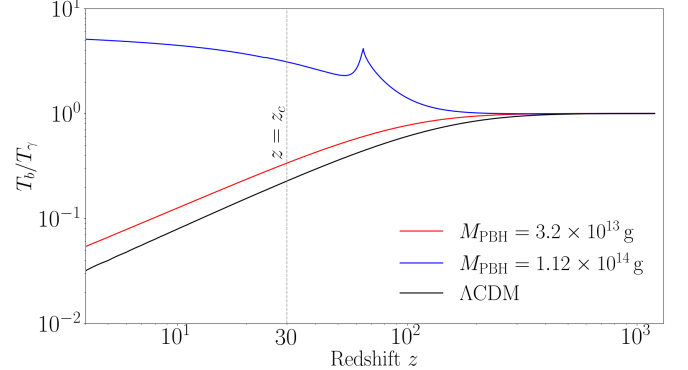


FIG. 5. Ratio of the baryon temperature T_b to the CMB photon temperature T_γ as a function of redshift. The black line shows the standard ΛCDM prediction. Colored lines include the effect of PBH evaporation for populations with masses $M_{\text{PBH}} = 3.2 \times 10^{13} \text{ g}$ (red) and $1.12 \times 10^{14} \text{ g}$ (blue), and corresponding initial abundances $\beta = 1.6 \times 10^{-27}$ and 1.4×10^{-26} .

sumptions about the astrophysical reionization history.

The impact on the thermal history is shown in Fig. 5, where the baryon temperature T_b is compared to the CMB photon temperature T_γ for the standard ΛCDM scenario and for the representative PBH population described above. As discussed below Eq. (12), baryons decouple from CMB photons already in the standard scenario. Energy injection from Hawking radiation does not alter the epoch of baryon–photon decoupling itself, but instead raises the baryon temperature after decoupling, partially compensating adiabatic cooling. As a result, the ratio T_b/T_γ is enhanced relative to the ΛCDM prediction, being systematically larger over a broad redshift range. This deviation gives a clear signature of exotic energy injection, distinct from the standard thermal history, with an amplitude that depends sensitively on the PBH mass and initial abundance. Such heating of the baryonic gas would also have direct implications for high-redshift 21-cm observables, so that future measurements of the IGM thermal state can be used jointly with reionization constraints.

Although incorporating small-scale temperature anisotropies (high- ℓ TT) would undoubtedly strengthen our constraints, we restrict our analysis to low- ℓ polarization data for robustness. PBH evaporation across the entire mass range considered here increases the total optical depth τ , leading to a global suppression of the CMB acoustic peaks by the screening factor $\exp(-2\tau)$. In addition, PBHs towards the lighter end of the mass range considered inject a significant amount of energy at high redshifts, increasing the post-recombination ionization fraction $X_e(z)$. This broadens the last scattering surface and enhances Silk damping, resulting in a characteristic suppression of the high- ℓ tail of the power spectrum, see e.g. Refs. [60–62]. As a consequence, including high- ℓ TT data would provide stricter limits across the entire PBH mass range, with particularly strong constraints for lighter PBHs, for which these

damping effects are most pronounced. However, extracting these constraints from high- ℓ data requires a full cosmological parameter inference to account for parameter degeneracies. The global suppression of the acoustic peaks is highly degenerate with the primordial scalar amplitude A_s through the combination $A_s \exp(-2\tau)$, while modifications to the damping tail can be degenerate with parameters governing standard recombination physics, such as the primordial helium abundance Y_P or the electron mass m_e [99]. Disentangling the PBH signal from these standard cosmological parameters requires a comprehensive and careful modeling of the parameter space. To avoid these model dependencies and the risk of parameter confusion, we rely exclusively on the low- ℓ EE polarization data. This approach yields a more conservative constraint that is driven purely by the reionization history reconstruction, accepting the trade-off of slightly weaker limits on the lightest PBHs in exchange for greater reliability and model independence.

A useful comparison for our reionization bounds is provided by constraints on PBH evaporation derived from CMB spectral distortions [63–68]. Spectral distortions are generated when EM energy is injected into the CMB after photon number-changing processes, such as double Compton scattering and bremsstrahlung, become inefficient, at redshifts $z \sim 10^4$ – 10^6 . Energy injection during this epoch produces departures from a blackbody spectrum, parametrized by the chemical potential μ and the Compton y parameter, which cannot be fully thermalized and are therefore tightly constrained by COBE/FIRAS (Cosmic Background Explorer-Far InfraRed Absolute Spectrophotometer) observations [100, 101]. By contrast, the analysis presented here focuses on the impact of PBH evaporation on the thermal and ionization history of the IGM at lower redshifts, $z \lesssim 800$, where injected energy primarily modifies the free-electron fraction and the baryon temperature rather than the CMB frequency spectrum. Although both approaches probe energy injection from PBH evaporation, they are sensitive to distinct physical observables: spectral-distortion measurements constrain early-time departures from a Planck CMB spectrum, while reionization constraints are driven by late-time changes in the ionization and thermal state of the gas. As a result, in the regime where PBH evaporation occurs predominantly at $z \sim 30$ – 800 , the reionization bounds derived here provide significantly stronger constraints. Future CMB spectral-distortion missions such as the Primordial Inflation Explorer (PIXIE) [102] and the Polarized Radiation Imaging and Spectroscopy Mission (PRISM) [103], together with improved high-redshift CMB polarization [104–107] and 21-cm measurements [108, 109], will provide complementary and substantially more sensitive probes of PBH evaporation across a wide range of redshifts and observables.

VI. CONCLUSIONS

In this work we have derived constraints on the initial abundance of evaporating primordial black holes (PBHs) using the reionization history of the Universe as a cosmological probe. We focused on PBHs with masses in the range $3.2 \times 10^{13} \text{ g} \lesssim M_{\text{PBH}} \lesssim 5 \times 10^{14} \text{ g}$, corresponding to BHs whose evaporation injects energy predominantly at redshifts below a benchmark value $z_{\text{max}} = 800$, chosen to ensure a clean separation from recombination physics. In this mass window, constraints from gamma-ray observations weaken, while the ionization and thermal histories of the intergalactic medium provide a sensitive and complementary probe of Hawking evaporation.

Our analysis introduces a state-of-the-art framework that combines a fully time-dependent treatment of PBH evaporation with a model-independent reconstruction of the reionization history. The Hawking emission spectra, including all Standard Model degrees of freedom and gravitons, are computed using `BlackHawk 2.3`, with final-state radiation modeled using `HAZMA`, while EM cascades and energy deposition into ionization, excitation, and heating are consistently tracked using `DarkHistory`. These effects are incorporated into a Gaussian Process reconstruction of the free-electron fraction based on low- ℓ CMB polarization data from *Planck* 2018 release, allowing us to constrain PBH evaporation through its contribution to the high-redshift optical depth, τ_{highz} , without relying on parametric assumptions about the reionization history. This approach allows for a well-defined separation between exotic energy injection at $z \gtrsim z_c \sim 30$, where the Universe is not expected to be fully reionized, and late-time astrophysical reionization. As a result, the derived bounds on the initial PBH abundance are robust against uncertainties in astrophysical modeling and directly trace the redshift-dependent impact of Hawking evaporation on the ionization history.

We find that reionization data place meaningful constraints on the initial PBH mass fraction β across the considered mass range, with a characteristic mass dependence driven by the timing and composition of the evaporated energy. For lighter PBHs, evaporation occurs closer to recombination, where an increasing fraction of the luminosity is carried by non-EM particles, leading to weaker constraints than estimates based on constant branching ratios. For heavier PBHs, evaporation proceeds at later times, when even modest EM energy injection can produce a pronounced enhancement in the free-electron fraction and a corresponding increase in the optical depth. Compared to earlier CMB anisotropy-based limits, our constraints are generally more conservative, reflecting the fully time-dependent and self-consistent treatment of evaporation, particle cascades, and energy deposition.

More broadly, this work shows the power of reionization as a precision probe of exotic energy injection in the early Universe when analyzed with flexible, data-driven techniques. Future improvements in large-scale

CMB polarization measurements, as well as forthcoming 21-cm observations, will significantly enhance sensitivity to deviations in the high-redshift ionization history and further strengthen constraints on PBH evaporation. The framework developed here is readily applicable to a wide class of scenarios involving unstable relics or late-time energy injection, providing a robust and model-independent pathway for testing new physics with cosmological data.

ACKNOWLEDGMENTS

We thank Doddy Marsh and Eleonora Di Valentino for helpful discussions and guidance on the implementation of the Gaussian Process reconstruction method and the handling of the data. LV also thanks Fabio

Iocco for useful suggestions. We acknowledge support by the National Natural Science Foundation of China (NSFC) through the grant No. 12350610240 “Astrophysical Axion Laboratories”. LV also acknowledges support by Istituto Nazionale di Fisica Nucleare (INFN) through the Commissione Scientifica Nazionale 4 (CSN4) Iniziativa Specifica “Quantum Universe” (QGSKY). LV thanks the Tsung-Dao Lee Institute for hospitality during the final stages of this work. This publication is based upon work from the COST Actions “COSMIC WIS-Pers” (CA21106) and “Addressing observational tensions in cosmology with systematics and fundamental physics (CosmoVerse)” (CA21136), both supported by COST (European Cooperation in Science and Technology). This work made use of the open source software matplotlib [110], numpy [111], and scipy [112].

[1] A. M. Ghez, B. L. Klein, M. Morris, and E. E. Becklin, *Astrophys. J.* **509**, 678 (1998), arXiv:astro-ph/9807210.

[2] A. M. Ghez et al., *Astrophys. J.* **689**, 1044 (2008), arXiv:0808.2870 [astro-ph].

[3] S. Gillessen, F. Eisenhauer, S. Trippe, T. Alexander, R. Genzel, F. Martins, and T. Ott, *Astrophys. J.* **692**, 1075 (2009), arXiv:0810.4674 [astro-ph].

[4] B. P. Abbott et al. (LIGO Scientific, Virgo), *Phys. Rev. Lett.* **116**, 061102 (2016), arXiv:1602.03837 [gr-qc].

[5] B. P. Abbott et al. (LIGO Scientific, Virgo), *Phys. Rev. X* **9**, 031040 (2019), arXiv:1811.12907 [astro-ph.HE].

[6] K. Akiyama et al. (Event Horizon Telescope), *Astrophys. J. Lett.* **875**, L1 (2019), arXiv:1906.11238 [astro-ph.GA].

[7] K. Akiyama et al. (Event Horizon Telescope), *Astrophys. J. Lett.* **930**, L12 (2022), arXiv:2311.08680 [astro-ph.HE].

[8] A. Heger, C. L. Fryer, S. E. Woosley, N. Langer, and D. H. Hartmann, *Astrophys. J.* **591**, 288 (2003), arXiv:astro-ph/0212469.

[9] Y. B. Zel'dovich and I. D. Novikov, *Sov. Astron.* **10**, 602 (1967).

[10] B. J. Carr and S. W. Hawking, *Mon. Not. Roy. Astron. Soc.* **168**, 399 (1974).

[11] B. J. Carr, *Astrophys. J.* **201**, 1 (1975).

[12] J. Garcia-Bellido, A. D. Linde, and D. Wands, *Phys. Rev. D* **54**, 6040 (1996), arXiv:astro-ph/9605094.

[13] C. T. Byrnes, M. Hindmarsh, S. Young, and M. R. S. Hawkins, *JCAP* **08**, 041 (2018), arXiv:1801.06138 [astro-ph.CO].

[14] D. N. Maeso, L. Marzola, M. Raidal, V. Vaskonen, and H. Veermäe, *JCAP* **02**, 017 (2022), arXiv:2112.01505 [astro-ph.CO].

[15] M. M. Flores and A. Kusenko, *Phys. Rev. Lett.* **126**, 041101 (2021), arXiv:2008.12456 [astro-ph.CO].

[16] S. W. Hawking, I. G. Moss, and J. M. Stewart, *Phys. Rev. D* **26**, 2681 (1982).

[17] H. Kodama, M. Sasaki, and K. Sato, *Prog. Theor. Phys.* **68**, 1979 (1982).

[18] M. Shibata and M. Sasaki, *Phys. Rev. D* **60**, 084002 (1999), arXiv:gr-qc/9905064.

[19] J. C. Niemeyer and K. Jedamzik, *Phys. Rev. D* **59**, 124013 (1999), arXiv:astro-ph/9901292.

[20] I. Musco, J. C. Miller, and L. Rezzolla, *Class. Quant. Grav.* **22**, 1405 (2005), arXiv:gr-qc/0412063.

[21] Y.-P. Wu, *Phys. Dark Univ.* **30**, 100654 (2020), arXiv:2005.00441 [astro-ph.CO].

[22] A. D. Gow, C. T. Byrnes, P. S. Cole, and S. Young, *JCAP* **02**, 002 (2021), arXiv:2008.03289 [astro-ph.CO].

[23] B. J. Carr, K. Kohri, Y. Sendouda, and J. Yokoyama, *Phys. Rev. D* **81**, 104019 (2010), arXiv:0912.5297 [astro-ph.CO].

[24] B. Carr, F. Kuhnel, and M. Sandstad, *Phys. Rev. D* **94**, 083504 (2016), arXiv:1607.06077 [astro-ph.CO].

[25] B. Carr, K. Kohri, Y. Sendouda, and J. Yokoyama, *Rept. Prog. Phys.* **84**, 116902 (2021), arXiv:2002.12778 [astro-ph.CO].

[26] B. Carr and F. Kuhnel, *Ann. Rev. Nucl. Part. Sci.* **70**, 355 (2020), arXiv:2006.02838 [astro-ph.CO].

[27] A. M. Green and B. J. Kavanagh, *J. Phys. G* **48**, 043001 (2021), arXiv:2007.10722 [astro-ph.CO].

[28] S. W. Hawking, *Nature* **248**, 30 (1974).

[29] H. Niikura et al., *Nature Astron.* **3**, 524 (2019), arXiv:1701.02151 [astro-ph.CO].

[30] B. J. Carr and M. Sakellariadou, *Astrophys. J.* **516**, 195 (1999).

[31] B. Carr, F. Kuhnel, and L. Visinelli, *Mon. Not. Roy. Astron. Soc.* **501**, 2029 (2021), arXiv:2008.08077 [astro-ph.CO].

[32] Y. Ali-Haïmoud and M. Kamionkowski, *Phys. Rev. D* **95**, 043534 (2017), arXiv:1612.05644 [astro-ph.CO].

[33] P. D. Serpico, V. Poulin, D. Inman, and K. Kohri, *Phys. Rev. Res.* **2**, 023204 (2020), arXiv:2002.10771 [astro-ph.CO].

[34] A. Coogan, L. Morrison, and S. Profumo, *Phys. Rev. Lett.* **126**, 171101 (2021), arXiv:2010.04797 [astro-ph.CO].

[35] C. Keith, D. Hooper, T. Linden, and R. Liu, *Phys. Rev. D* **106**, 043003 (2022), arXiv:2204.05337 [astro-ph.HE].

[36] T. Fujita, M. Kawasaki, K. Harigaya, and R. Matsuda, *Phys. Rev. D* **89**, 103501 (2014), arXiv:1401.1909 [astro-ph.CO].

[37] R. Allahverdi, J. Dent, and J. Osinski, *Phys. Rev. D* **97**, 055013 (2018), arXiv:1711.10511 [astro-ph.CO].

[38] O. Lennon, J. March-Russell, R. Petrossian-Byrne, and H. Tillim, *JCAP* **04**, 009 (2018), arXiv:1712.07664 [hep-ph].

[39] L. Morrison, S. Profumo, and Y. Yu, *JCAP* **05**, 005 (2019), arXiv:1812.10606 [astro-ph.CO].

[40] D. Hooper, G. Krnjaic, and S. D. McDermott, *JHEP* **08**, 001 (2019), arXiv:1905.01301 [hep-ph].

[41] I. Masina, *Eur. Phys. J. Plus* **135**, 552 (2020), arXiv:2004.04740 [hep-ph].

[42] A. Cheek, L. Heurtier, Y. F. Perez-Gonzalez, and J. Turner, *Phys. Rev. D* **105**, 015023 (2022), arXiv:2107.00016 [hep-ph].

[43] P. Chattopadhyay, A. Chaudhuri, and M. Y. Khlopov, *Int. J. Geom. Meth. Mod. Phys.* **22**, 2450251 (2025), arXiv:2209.11288 [hep-ph].

[44] K. Mazde and L. Visinelli, *JCAP* **01**, 021 (2023), arXiv:2209.14307 [astro-ph.CO].

[45] I. Baldes, Q. Decant, D. C. Hooper, and L. Lopez-Honorez, *JCAP* **08**, 045 (2020), arXiv:2004.14773 [astro-ph.CO].

[46] P. Gondolo, P. Sandick, and B. Shams Es Haghi, *Phys. Rev. D* **102**, 095018 (2020), arXiv:2009.02424 [hep-ph].

[47] S. M. Boucenna, F. Kuhnel, T. Ohlsson, and L. Visinelli, *JCAP* **07**, 003 (2018), arXiv:1712.06383 [hep-ph].

[48] G. Bertone, A. M. Coogan, D. Gaggero, B. J. Kavanagh, and C. Weniger, *Phys. Rev. D* **100**, 123013 (2019), arXiv:1905.01238 [hep-ph].

[49] M. P. Hertzberg, E. D. Schiappacasse, and T. T. Yanagida, *Phys. Rev. D* **102**, 023013 (2020), arXiv:2001.07476 [astro-ph.CO].

[50] B. Carr, F. Kuhnel, and L. Visinelli, *Mon. Not. Roy. Astron. Soc.* **506**, 3648 (2021), arXiv:2011.01930 [astro-ph.CO].

[51] E. U. Ginés, O. Mena, and S. J. Witte, *Phys. Rev. D* **106**, 063538 (2022), arXiv:2207.09481 [astro-ph.CO].

[52] P. Chanda, J. Scholtz, and J. Unwin, *JHEP* **07**, 273 (2024), arXiv:2209.07541 [hep-ph].

[53] G. Bertone, A. R. A. C. Wierda, D. Gaggero, B. J. Kavanagh, M. Volonteri, and N. Yoshida, *Phys. Rev. D* **112**, 043537 (2025), arXiv:2404.08731 [astro-ph.CO].

[54] P. Jangra, D. Gaggero, B. J. Kavanagh, and J. M. Diego, *JCAP* **08**, 006 (2025), arXiv:2412.11921 [astro-ph.CO].

[55] A. Boccia, F. Iocco, and L. Visinelli, *Phys. Rev. D* **111**, 063508 (2025), arXiv:2405.18493 [astro-ph.CO].

[56] X.-L. Chen and M. Kamionkowski, *Phys. Rev. D* **70**, 043502 (2004), arXiv:astro-ph/0310473.

[57] N. Padmanabhan and D. P. Finkbeiner, *Phys. Rev. D* **72**, 023508 (2005), arXiv:astro-ph/0503486.

[58] T. R. Slatyer, N. Padmanabhan, and D. P. Finkbeiner, *Phys. Rev. D* **80**, 043526 (2009), arXiv:0906.1197 [astro-ph.CO].

[59] T. R. Slatyer, *Phys. Rev. D* **93**, 023527 (2016), arXiv:1506.03811 [hep-ph].

[60] V. Poulin, J. Lesgourges, and P. D. Serpico, *JCAP* **03**, 043 (2017), arXiv:1610.10051 [astro-ph.CO].

[61] P. Stöcker, M. Krämer, J. Lesgourges, and V. Poulin, *JCAP* **03**, 018 (2018), arXiv:1801.01871 [astro-ph.CO].

[62] H. Poulter, Y. Ali-Haïmoud, J. Hamann, M. White, and A. G. Williams, (2019), arXiv:1907.06485 [astro-ph.CO].

[63] H. Tashiro and N. Sugiyama, *Phys. Rev. D* **78**, 023004 (2008), arXiv:0801.3172 [astro-ph].

[64] J. Chluba and D. Grin, *Mon. Not. Roy. Astron. Soc.* **434**, 1619 (2013), arXiv:1304.4596 [astro-ph.CO].

[65] J. Chluba et al., *Exper. Astron.* **51**, 1515 (2021), arXiv:1909.01593 [astro-ph.CO].

[66] M. Lucca, N. Schöneberg, D. C. Hooper, J. Lesgourges, and J. Chluba, *JCAP* **02**, 026 (2020), arXiv:1910.04619 [astro-ph.CO].

[67] S. K. Acharya and R. Khatri, *JCAP* **02**, 010 (2020), arXiv:1912.10995 [astro-ph.CO].

[68] S. K. Acharya and R. Khatri, *JCAP* **06**, 018 (2020), arXiv:2002.00898 [astro-ph.CO].

[69] S. Clark, B. Dutta, Y. Gao, Y.-Z. Ma, and L. E. Strigari, *Phys. Rev. D* **98**, 043006 (2018), arXiv:1803.09390 [astro-ph.HE].

[70] J. Mirocha, P. La Plante, and A. Liu, *Mon. Not. Roy. Astron. Soc.* **507**, 3872 (2021), arXiv:2012.09189 [astro-ph.CO].

[71] H. Cheng, Z. Yin, E. Di Valentino, D. J. E. Marsh, and L. Visinelli, (2025), arXiv:2506.19096 [astro-ph.CO].

[72] Z. Yin, H. Cheng, E. Di Valentino, N. Gendler, D. J. E. Marsh, and L. Visinelli, (2025), arXiv:2507.03535 [hep-ph].

[73] S. W. Hawking, *Commun. Math. Phys.* **43**, 199 (1975), [Erratum: Commun.Math.Phys. 46, 206 (1976)].

[74] D. N. Page and S. W. Hawking, *Astrophys. J.* **206**, 1 (1976).

[75] B. J. Carr, *Astrophys. J.* **206**, 8 (1976).

[76] T. Harada, C.-M. Yoo, K. Kohri, and K.-I. Nakao, *Phys. Rev. D* **96**, 083517 (2017), [Erratum: Phys.Rev.D 99, 069904 (2019)], arXiv:1707.03595 [gr-qc].

[77] V. De Luca, V. Desjacques, G. Franciolini, A. Malhotra, and A. Riotto, *JCAP* **05**, 018 (2019), arXiv:1903.01179 [astro-ph.CO].

[78] S. A. Teukolsky, *Astrophys. J.* **185**, 635 (1973).

[79] J. M. Bardeen and W. H. Press, *J. Math. Phys.* **14**, 7 (1973).

[80] J. H. MacGibbon and B. R. Webber, *Phys. Rev. D* **41**, 3052 (1990).

[81] J. H. MacGibbon, *Phys. Rev. D* **44**, 376 (1991).

[82] A. Arbey and J. Auffinger, *Eur. Phys. J. C* **79**, 693 (2019), arXiv:1905.04268 [gr-qc].

[83] A. Arbey and J. Auffinger, *Eur. Phys. J. C* **81**, 910 (2021), arXiv:2108.02737 [gr-qc].

[84] J. Auffinger and A. Arbey, *PoS CompTools2021*, 017 (2022), arXiv:2207.03266 [gr-qc].

[85] A. Coogan, L. Morrison, and S. Profumo, *JCAP* **01**, 056 (2020), arXiv:1907.11846 [hep-ph].

[86] M. Escudero, C. K. Pooni, M. Fairbairn, D. Blas, X. Du, and D. J. E. Marsh, *Phys. Rev. D* **109**, 043018 (2024), arXiv:2302.10206 [hep-ph].

[87] T. R. Slatyer and C.-L. Wu, *Phys. Rev. D* **95**, 023010 (2017), arXiv:1610.06933 [astro-ph.CO].

[88] H. Liu, G. W. Ridgway, and T. R. Slatyer, *Phys. Rev. D* **101**, 023530 (2020), arXiv:1904.09296 [astro-ph.CO].

[89] S. Galli, F. Iocco, G. Bertone, and A. Melchiorri, *Phys. Rev. D* **84**, 027302 (2011), arXiv:1106.1528 [astro-ph.CO].

[90] S. Galli, T. R. Slatyer, M. Valdes, and F. Iocco, *Phys. Rev. D* **88**, 063502 (2013), arXiv:1306.0563 [astro-ph.CO].

[91] D. P. Finkbeiner, S. Galli, T. Lin, and T. R. Slatyer, *Phys. Rev. D* **85**, 043522 (2012), arXiv:1109.6322 [astro-ph.CO].

[92] T. R. Slatyer, *Phys. Rev. D* **87**, 123513 (2013),

arXiv:1211.0283 [astro-ph.CO].

[93] B. D. Fields, K. A. Olive, T.-H. Yeh, and C. Young, *JCAP* **03**, 010 (2020), [Erratum: *JCAP* 11, E02 (2020)], arXiv:1912.01132 [astro-ph.CO].

[94] C. Heinrich and W. Hu, *Phys. Rev. D* **104**, 063505 (2021), arXiv:2104.13998 [astro-ph.CO].

[95] N. Aghanim et al. (Planck), *Astron. Astrophys.* **641**, A1 (2020), arXiv:1807.06205 [astro-ph.CO].

[96] N. Aghanim et al. (Planck), *Astron. Astrophys.* **641**, A5 (2020), arXiv:1907.12875 [astro-ph.CO].

[97] J. Torrado and A. Lewis, *JCAP* **05**, 057 (2021), arXiv:2005.05290 [astro-ph.IM].

[98] D. Blas, J. Lesgourgues, and T. Tram, *JCAP* **07**, 034 (2011), arXiv:1104.2933 [astro-ph.CO].

[99] N. Aghanim et al. (Planck), *Astron. Astrophys.* **641**, A6 (2020), [Erratum: *Astron. Astrophys.* 652, C4 (2021)], arXiv:1807.06209 [astro-ph.CO].

[100] D. J. Fixsen, E. S. Cheng, J. M. Gales, J. C. Mather, R. A. Shafer, and E. L. Wright, *Astrophys. J.* **473**, 576 (1996), arXiv:astro-ph/9605054.

[101] D. J. Fixsen and J. C. Mather, *Astrophys. J.* **581**, 817 (2002).

[102] A. Kogut et al., *JCAP* **07**, 025 (2011), arXiv:1105.2044 [astro-ph.CO].

[103] P. André et al. (PRISM), *JCAP* **02**, 006 (2014), arXiv:1310.1554 [astro-ph.CO].

[104] P. Ade et al. (Simons Observatory), *JCAP* **02**, 056 (2019), arXiv:1808.07445 [astro-ph.CO].

[105] E. Ally et al. (LiteBIRD), *PTEP* **2023**, 042F01 (2023), arXiv:2202.02773 [astro-ph.IM].

[106] N. Sehgal et al., *Bull. Am. Astron. Soc.* **51**, 1 (2019), arXiv:1906.10134 [astro-ph.CO].

[107] S. Aiola et al. (CMB-HD), (2022), arXiv:2203.05728 [astro-ph.CO].

[108] S. Munshi et al., *Astron. Astrophys.* **681**, A62 (2024), arXiv:2311.05364 [astro-ph.CO].

[109] Z. Abdurashidova et al. (HERA), (2025), arXiv:2511.21289 [astro-ph.CO].

[110] J. D. Hunter, *Computing in Science and Engineering* **9**, 90 (2007).

[111] C. R. Harris et al., *Nature (London)* **585**, 357 (2020), arXiv:2006.10256 [cs.MS].

[112] P. Virtanen et al., *Nature Methods* **17**, 261 (2020), arXiv:1907.10121 [cs.MS].